Vertical Single-Wall Carbon Nanotube Forests as Plasmonic Heat Pipes

Andrei M. Nemilentsau[†,*] and Slava V. Rotkin[†,‡,*]

[†]Department of Physics, Lehigh University, 16 Memorial Drive East, Bethlehem, Pennsylvania 18015, United States and [‡]Center for Advanced Materials and Nanotechnology, Lehigh University, 5 East Packer Avenue, Bethlehem, Pennsylvania 18015, United States

ABSTRACT

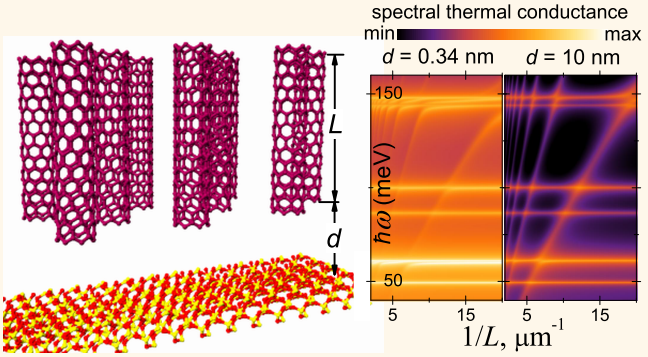

High thermal conductivity of carbon nanotubes (NTs) is attractive for the heat removal applications. However, the problem of efficient thermal coupling to the heater/cooler still needs to be resolved. We study near-field electromagnetic tunneling as a mechanism of heat transfer across the interface. We report interface thermal (Kapitza) conductance between a low-density vertical metallic single-wall NT forest and a quartz substrate on the order of 50 MW/Km^2 and explain it by strong electromagnetic interaction and near-field entanglement between the surface phonon–polaritons in the polar dielectric and the NT plasmons. We predict that the thickness of the NT film can be tweaked to the resonance wavelength of these entangled modes for performance optimization of nanocarbon thermal interconnects.

KEYWORDS: interface thermal conductance · Kapitza conductance · near-field heat · single-wall nanotubes · surface polariton

Cost-efficient management of the heat generated in integrated circuits is one of the grand challenges of contemporary electronics.[1] A solution to this problem is further perplexed by the high density of dissipated power. Thus development of new resilient heat conducting materials is increasingly important. High strength, flexibility, and intrinsic thermal conductivity of carbon nanotubes (NTs) make materials on their basis attractive for thermal management applications.[2] However, apart from the high intrinsic conductivity, an efficient coupling of NT materials to heater and cooler reservoir, that is, a high contact, or Kapitza, conductance is also required.

Recently, thermal transport through individual NTs[3−10] and NT arrays[11−17] was shown to be dominated by a high thermal resistance at the interface. The reported values for the interface thermal conductivity vary significantly from sample to sample. Particularly, for an interface between metallic single-wall carbon nanotubes (SWNT) and quartz, these values are in the range from 0.007 to 0.17 W m^{-1} K^{-1}, spanning more than 1 order of magnitude.[5−7] Thus, further studies of the mechanisms responsible for the thermal interface coupling should be indispensable for understanding both the origin of these variations and ways to enhance the Kapitza conductivity.

One of the mechanisms, providing a substantial contribution to the interface thermal conductivity, is direct phonon heat transport. Such a transport between NTs and various substrates/media was studied in refs 18−24. However, the earlier works often neglected the role or underestimated the importance of the electromagnetic radiation. Here it will be shown to contribute significantly to the heat transfer across the interface. It was first predicted by Polder and Van Hove[25] that the heat transport across the vacuum gap between two macroscopic bodies dramatically increases when the gap width becomes smaller than the thermal radiation wavelength because of increasing contribution of the nonpropagating evanescent modes. Since then, the importance of the near-field electromagnetic mode tunneling across the vacuum gap for the thermal coupling has been both studied theoretically[26−31] and demonstrated experimentally[32−34] for a number of different systems, including the SiO_2–graphene interface.[30]

In this article, we focus on the near-field radiative heat transfer between a vertical forest of metallic SWNTs and a polar (SiO_2) substrate. Not only can such a system be achieved experimentally and applied for thermal solutions, but it also demonstrates an

* Address correspondence to ann311@lehigh.edu, rotkin@lehigh.edu.

Received for review February 27, 2012 and accepted April 5, 2012.

Published online April 05, 2012
10.1021/nn300848b

interesting fundamental physics effect, such as polariton localization and near-field plasmon–polariton entanglement (to be discussed below). Using the formalism of the fluctuation electrodynamics,[35] we predict the high magnitude of the near-field Kapitza conductance. By analyzing spectral function of Kapitza conductance, we will identify the origin of such a high interface thermal coupling, which is the strong electromagnetic interaction between surface phonon–polaritons in the polar dielectric (substrate) and plasmons in the SWNT. We will present dependence of the Kapitza conductance on the vacuum gap, which shows a power law with two characteristic length scales. All of these data will be explained in terms of the (quantum) electrodynamic coupling of the surface modes. Since the properties of those modes can be controlled experimentally, we make the predictions on the optimization of performance of the SWNT forest thermal interconnects.

RESULTS AND DISCUSSION

The Model. Two main conditions for the near-field heat exchange becoming a dominating thermal conductance mechanism are (i) (relatively) small interface gap, on the order of several nanometers, as we show next, and (ii) resonance coupling of the electromagnetic modes of two surfaces. For the polar substrate, such modes are the surface phonon–polaritons,[36] and for the SWNT forest, these could be either one-electron excitations or the collective modes, plasmons. The former will be studied elsewhere, and the latter, plasmons, known to have a large oscillator strength, are the subject of our current study. As we justify below, the efficiency of plasmon–polariton coupling is so high for the SWNT forest directly applied to the quartz surface that even a moderate forest density allows one to achieve a good heat exchange rate. Thus, in what follows, we assume the forest to be sufficiently rarefied, so that the mutual electromagnetic interaction between SWNTs can be neglected. This can be achieved for average distance between the SWNTs exceeding a few tens of nanometers,[37] that is, for the forest density N smaller than 10^{16} m^{-2}.

We also assume, for the sake of clarity, that the vertical forest solely consists of identical metallic SWNTs of length L, placed at a distance d above semi-infinite polar dielectric substrate (Figure 1 inset) with the known dielectric function $\varepsilon_{sub}(\omega)$, absorbing and isotropic homogeneous. One can show that the variation of the near-field Kapitza conductance between the forest and the substrate upon changing the SWNT radius is negligible (see Supporting Information). We discuss the role of nonmetallic NTs and the length dependence later. The SWNTs in the forest are assumed to be "free standing", that is, in vacuum (air). Heat leak from SWNTs in the air can be neglected as compared to heat transport along SWNTs because of the

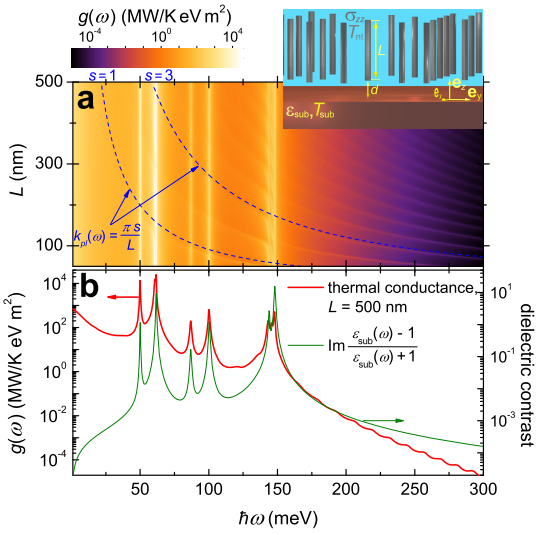

Figure 1. (a) Spectral Kapitza conductance, $g(\omega)$, between quartz substrate and vertical forest of (15,0) SWNTs, at $N = 10^{16}$ m^{-2}, $d = 3.4$ Å, $T_{sub} = 300$ K, as a function of the SWNT length, L, and the frequency. Blue lines follow the analytic dispersion for plasmons: $k_{pl} = \pi s/L$. (b) Cross section of $g(\omega)$ at $L = 500$ nm (red line), and dielectric contrast for the quartz–air interface (green line) as a function of frequency. (Inset) Schematic geometry of the thermal interface.

small value of thermal Kapitza conductance at the SWNT–air interface (10^3–10^5 W m^{-2} K^{-1}).[38,39] Therefore, we assume that local thermal equilibrium at a given temperature is set within each SWNT.

Within an approximation of noncoupled plasmons and following the fluctuation electrodynamics formalism established by Rytov,[35] the radiative heat flux between the SWNT forest and the dielectric substrate at a given frequency, ω, that is the heat spectral density can be written as (see Methods section for details)

$$\dot{q}(\omega) = \frac{N\omega^3 \mathrm{Re}\sigma_{zz}(\omega)\,\mathrm{Im}\varepsilon_{sub}(\omega)}{2\pi^2 c^4}(\Theta(\omega, T_{sub}) - \Theta(\omega, T_{nt})) \times \int_{S_{nt}} d\mathbf{R}_{nt} \int_{V_{sub}} d\mathbf{R}_{sub} \sum_{\alpha = x,y,z} |G_{\alpha z}(\mathbf{R}_{sub}, \mathbf{R}_{nt}, \omega)|^2 \quad (1)$$

where $\Theta(\omega,T) = \hbar\omega/(\exp(\hbar\omega/k_BT) - 1)$ is the blackbody thermal function, $\sigma_{zz}(\omega)$ is the axial linear surface conductivity of a metallic SWNT, k_B is the Boltzmann constant, c is the speed of light in the vacuum, and $\mathbf{R}_{sub}$, $\mathbf{R}_{nt}$ are the radius vectors of the points in the substrate volume V_{sub} and on the SWNT surface S_{nt}, respectively. Here we assume that both the substrate and SWNTs in the forest are in their local thermodynamic equilibrium at temperatures T_{sub} and T_{nt}, respectively. In order to calculate the electric Green dyadic of $G_{\alpha z}(\mathbf{R}_{sub},\mathbf{R}_{nt},\omega)$ of an individual metallic SWNT placed above the substrate, we apply the numerical approach developed in our previous works[40–42] (see Methods section for details).

Simulation Results. We restrict our consideration to the low-frequency range, well below frequencies of the

interband electron transitions in metallic SWNTs, as it provides the main contribution to the heat flux (see Figure 1). The conductivity of the metallic SWNT in this range is of Drude type[43,44]

$$\sigma_{zz}(\omega) = i\frac{2v_F e^2}{\pi^2 R\hbar(\omega + i/\tau)} \quad (2)$$

where $v_F \approx 8 \times 10^7$ cm s^{-1} is the Fermi velocity in SWNT or graphene, e is the electron charge, $\hbar$ is the reduced Planck constant, R is the SWNT radius, and $\tau \sim 100$ fs is the relaxation time. The quartz dielectric function is parametrized as in refs 45 and 46. The spectrum of the imaginary part of the dielectric contrast at the quartz−air interface, $\mathrm{Im}(\varepsilon_{sub}(\omega) - 1)/(\varepsilon_{sub}(\omega) + 1)$, is presented as a green line in Figure 1b. It contains six resonance lines[47] which are the surface phonon−polaritons (SPP), defined by the condition

$$\mathrm{Re}\varepsilon_{sub}(\omega_{SPP}) = -1 \quad (3)$$

The spectral Kapitza conductance, $g(\omega) = \lim_{T_{sub}\to T_{nt}} \dot{q}(\omega)/(T_{sub} - T_{nt})$, of the forest of identical metallic (15,0) SWNTs with the forest density $N = 10^{16}$ m^{-2}, placed at the minimum (van der Waals) distance $d = 3.4$ Å above the quartz substrate surface at the temperature $T_{sub} = 300$ K, is plotted in Figure 1a. Two families of pronounced resonances can be found on the density plot. The frequencies of the bright vertical resonances do not depend on the SWNT length and coincide with the resonances of the dielectric contrast (green line in Figure 1b). Thus the origin of these resonances is the polaritons in quartz. The frequencies of the resonances of the second family (faded orange curves in Figure 1a) decrease with the SWNT length according to the simple power law which is understood as the space-quantization of the plasmons in a SWNT of a finite length:[48,49]

$$\omega_{pl} \propto k_{pl} \approx \frac{\pi s}{L} \quad (4)$$

such approximately linear dispersion of the plasmons was numerically obtained in ref 43, where s is an integer (quantum) number. We found this analytic dispersion relation (blue lines in Figure 1a) to be in very good agreement with the maxima corresponding to plasmon resonances in $g(\omega)$. Such plasmon resonances also reveal themselves in the spectra of thermal radiation from metallic SWNTs.[40]

The spectral Kapitza conductance, $g(\omega)$, is peaked at the frequencies of the polariton resonances in quartz and decreases fast at higher frequencies: for example, at $\hbar\omega = 60$ meV (at the second polariton resonance frequency), $g(\omega)$ is more than 8 orders of magnitude higher than at $\hbar\omega = 300$ meV. This is due to the spectral density of the electromagnetic modes, proportional to the imaginary part of the dielectric contrast, decreases as $1/\omega^3$, and, most importantly, the equilibrium thermal function $\Theta(\omega,T)$ decreases exponentially with ω. When the polariton energy exceeds the thermal energy $k_BT \approx 26$ meV, the spectral contribution to the total heat flux becomes negligible (at room temperature).

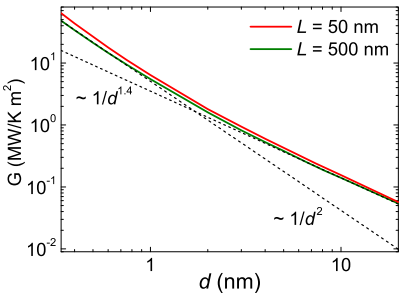

Figure 2. Total Kapitza conductance, G, as a function of the gap width d at $T_{sub} = 300$ K, $N = 10^{16}$ m^{-2}, for $L = 50$, 500 nm forest thickness (top red and lower green curves).

The spectral Kapitza conductance, $g(\omega)$, is almost independent of the SWNTs length L and decreases monotonously with the separation distance, d, and so does the total Kapitza conductance $G = \int_0^\infty g(\omega)\mathrm{d}\omega$ (Figure 2). It falls rapidly with increasing gap width, in particular, the Kapitza conductance across the 10 nm gap is more than 30 times smaller than across the 1 nm gap. However, we emphasize that the phonon heat conductance will be zero at the gap exceeding the amplitude of the thermal motion of individual atoms (bond length), which is about several angstroms, so the near-field Kapitza conductance wins over all other "contact" mechanisms if the substrate surface is rough. Furthermore, for the gap narrower than 1 nm, the Kapitza conductance decreases as $1/d^2$, while the decrease rate is slowing down for larger distance. It should be noted that a similar gap width dependence (with different characteristic distances and decay rates) of the thermal near-field Kapitza conductance was demonstrated for sphere−plate[32] and plate−plate[34,50,51] geometries. This behavior reflects the spatial structure of the electrical near-field in the gap between the plane substrate and SWNT.

Data Analysis and Interpretation. Although the physical picture of the near-field heat flux supported by two types of surface polariton modes (of the SWNT and of the quartz) is consistent with our data, careful examination of the spectral function $g(\omega)$ reveals additional peaks, not present in the dielectric contrast of quartz and different from the plasmon family (compare red and green curves in the vicinity of the surface phonon resonances in Figure 1b, at frequencies 60, 144, and 148 meV). One can clearly resolve doublet resonance lines in the Kapitza conductance spectrum, with the lower term of the doublet laying below the quartz surface phonon−polariton. In order to study this doublet splitting in more detail, we present magnified maps of the spectral Kapitza conductance in Figure 3 for different gap width d. The frequency region in Figure 3 (40 meV $\leq \hbar\omega \leq$ 160 meV) covers all six polaritons of quartz.

The maximum of $g(\omega,k)$ reveals the dispersion of all electromagnetic modes of the system, as a function of

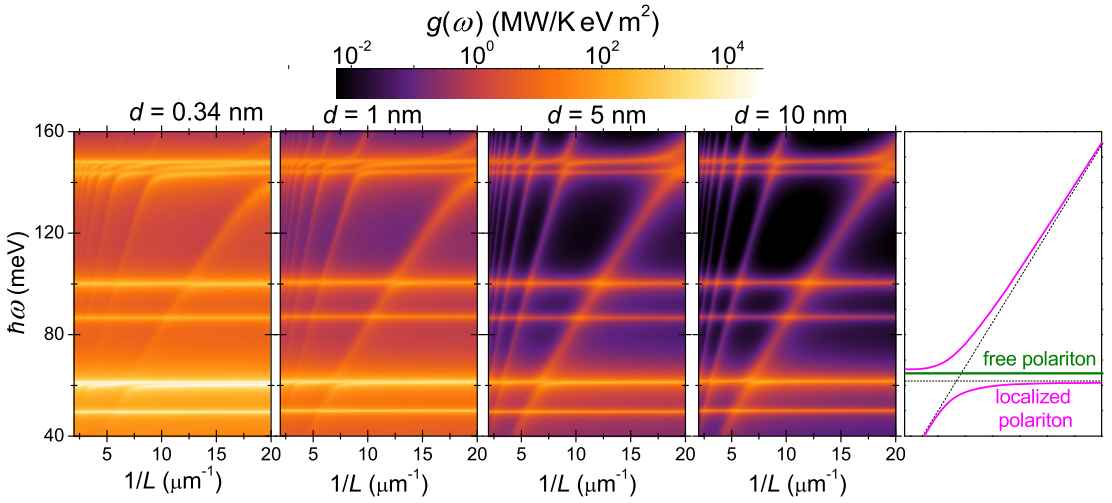

Figure 3. Spectral Kapitza conductance as a function of the inverse SWNT length, 1/*L* (quantized plasmon momentum), and the frequency for different gap widths *d*, as indicated in the legend, at $T_{sub} = 300$ K, $N = 10^{16}$ m^{-2}. Schematic representation of the polariton line splitting is presented in the rightmost panel.

SPP frequency and momentum or plasmon frequency and (quantized) momentum, which is proportional to the reciprocal SWNT length: $k_{pl} \propto L^{-1}$, according to eq 4. Anticrossing of the plasmon and phonon–polariton modes is clearly seen in Figure 3. Thus, in the narrow region—at the interception of the horizontal lines of the SPP modes (without dispersion) and the (linear dispersion) lines of the plasmons—where $\omega_{SPP} \simeq \omega_{pl}$, these two modes should be entangled. In addition to the entangled modes, one can resolve a nondispersion (SPP-like) mode which does not couple to the plasmon, as schematically shown in the right panel of Figure 3. Physics of the doublet is understood by comparing different panels of Figure 3. We note that the splitting (coupling) of the polariton resonances decreases with the gap width, and for 10 nm gap, the splitting can hardly be seen at all. At the same time, the noncoupled resonance is preserved at the same frequency in all panels. We conclude that the latter peak is due to the bare SPP modes of the quartz substrate, while the former mode is a localized polariton. Despite the fact that the SWNT cross section is much smaller than the wavelength of the phonon–polaritons, the polarization interaction between the plasmon and SPP modes can lead to the localization of the polaritons in the closest proximity of the SWNT, where the strength of the interaction is largest. Localized (bound) polaritons should have the energy below the nonlocalized (continuum) SPP modes, consistent with the numerical data.

Thermal Efficiency and Performance Optimization. Now we have identified all of the spectral features of $g(\omega,k)$ and are able to analyze performance of the SWNT thermal interconnects as a function of the sample thickness and density. In order to compare the interconnect with the current thermal management technologies, we estimate the heat generation density of a modern

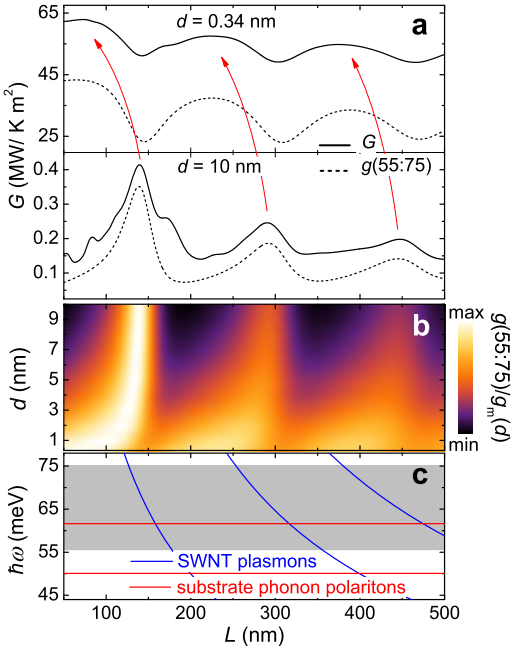

Figure 4. (a) Kapitza conductance, *G*, as a function of SWNTs length *L* for two different gap widths, *d*, between the forest of (15,0) SWNTs and the quartz substrate. Dashed lines denote the Kapitza conductance $g(\omega_1{:}\omega_2) = \int_{\omega_1}^{\omega_2} g(\omega) d\omega$ in the frequency range from ω_1 to ω_2. (b) Normalized conductance *g*(55:75) as a function of *d* and *L*. The normalization function $g_m(d)$ is defined as a maximum value of *g*(55:75) for a given *d*. (c) Blue and red lines are the solutions of eq 4 for surface plasmons in the SWNT and eq 3 for polaritons in quartz, correspondingly.

electronics chip at the level of 1 MW m^{-2}. For a typical temperature drop of 100 K between the hot and cold sides of the film, one needs $G \sim 10^{-2}$ MW K^{-1} m^{-2}, which is exceeded by more than 3 orders of magnitude by the predicted near-field efficiency of the SWNT forest with the moderate density $N = 10^{16}$ m^{-2}, which *post factum* justifies viability of our model assumption of a noninteracting low-density NT array. We note that

the semiconducting NT at zero doping level does not support low-frequency plasmons and, thus, will be inactive/inefficient in the heat transport in our model (see Supporting Information). However, in reality, all SWNTs have unintentional hole doping, thus in the SWNT forest, most of the NT channels will be active.

The thickness dependence of the Kapitza conductance is nonmonotonous (Figure 4), which further allows material optimization. Three broad maxima (major peaks superimposed by a number of smaller peaks) can be seen in Figure 4a in the Kapitza conductance of the forest as a function of the film thickness between 50 and 500 nm. We note that the top curves are shown for $d = 0.34$ nm and demonstrate much larger broadening as well as the peak shift to the smaller L as compared to $d = 10$ nm (bottom curves). Solid and dashed curves show the total Kapitza conductance and the partial Kapitza conductance.[52] Figure 4a shows that the partial conductance (the integral in the narrow vicinity of the strongest SPP peak, 55 meV $\leq \hbar\omega \leq$ 75 meV, shaded in panel c) constitutes most of the total Kapitza conductance. This partial Kapitza conductance consists of only one peak (single coupled polariton mode) and allows a simple interpretation.

Panel b shows corresponding partial conductance $g(55{:}75)$ as a function of both the film thickness and the gap width. The forest thickness, L_{max}, corresponding to the conductance maximum, is close to the value at interception of the first three plasmon resonances with second polariton in quartz (Figure 4c). It should be mentioned that eq 4, strictly speaking, defines the plasmon resonances for the SWNT in vacuum. Interaction between the plasmons in the SWNT and the polaritons in the substrate leads to the red shift of the plasmon resonances as well as to their broadening. This red shift reveals itself as "bending" of the curve of $L_{max}(d)$ in panels a and b at small d.

It is instructive to derive the Kapitza conductance between an individual SWNT in the forest and the substrate per unit of the SWNT−interface contact area: $g_{nt} = G/N\pi R^2$. Taking into account that Kapitza conductance G across the 5 nm gap between the forest of metallic (15,0) SWNTs of length $L = 500$ nm, at $N = 10^{16}$ m^{-2}, is equal to 0.38 MW K^{-1} m^{-2} and taking $R = 0.59$ nm, we obtain a typical value $g_{nt} = 3.4 \times 10^7$ W K^{-1} m^{-2}, which is in a good agreement with the experimental value presented in ref 5.

Finally, we compare phonon heat transport across the interface with the plasmon mechanism. The phonon−phonon contribution to the thermal Kapitza conductance g_{nt} across the 2.2 Å gap between a short (3.69 nm in length) armchair (10,10) SWNT and a SiO_2 substrate was estimated in ref 23 to be 5.8×10^7 W m^{-2} K^{-1}. We calculated the plasmon contribution across the 3.4 Å gap between a short (50 nm in length) zigzag (15,0) metallic SWNT[53] and SiO_2 substrate to be 570×10^7 W m^{-2} K^{-1}. This contribution gradually decreases as the gap width increases to 100 Å to the value 1.4×10^7 W m^{-2} K^{-1}. However, at this gap, the phonon mechanism would give zero value for Kapitza conductance. Thus we conclude that the plasmon thermal coupling mechanism clearly dominates the phonon mechanism in this geometry.

CONCLUSIONS

Concluding, in this work, using the methods of the fluctuation electrodynamics, we numerically calculated the near-field component of the heat transfer between the polar substrate and the NT thermal interconnect. For the vertical SWNT forest of a low density, we demonstrate theoretically that the electromagnetic near-field contribution to the interfacial Kapitza conductance is on the order of 50 MW K^{-1} m^{-2}, comparable or larger than the classical phonon contribution. Moreover, in contrast to phonon contribution, we proposed a "noncontact" heat conduction mechanism, decaying as $1/d^{\alpha}$ with the vacuum gap between the edge of the SWNT forest at the substrate surface, where $\alpha \sim 1.5-2$. The spectral analysis of the Kapitza conductance revealed the existence of entangled surface phonon−plasmon−polariton modes that are responsible for the strong near-field coupling across the vacuum gap. We predict that the performance optimization is possible for the interconnects, by tweaking the thickness of the SWNT film to the resonance with the wavelength of the entangled polariton modes.

METHODS

The heat flux between a rarefied vertical forest of plasmonically uncoupled metallic SWNTs and dielectric substrate is given by

$$\dot{Q} \approx N(P^{\text{sub}\rightarrow\text{nt}} - P^{\text{nt}\rightarrow\text{sub}}) \quad (5)$$

where the first term

$$P^{\text{sub}\rightarrow\text{nt}} = \int_{S_{nt}} d\mathbf{R}_{nt} \langle \mathbf{j}^{\text{in, sub}}(\mathbf{R}_{nt}, t) \cdot \mathbf{E}^{\text{sub}}(\mathbf{R}_{nt}, t) \rangle \quad (6)$$

is the electromagnetic power transferred from the (hot) substrate to each of individual SWNTs, $\mathbf{j}^{\text{in,sub}}$ is the electric current density induced on the SWNT surface, S_{nt}, by the electric field $\mathbf{E}^{\text{sub}}$ of the fluctuating currents in the substrate, $\mathbf{j}^{\text{sub}}$, and the angular brackets denote statistical ensemble average. The second term gives the electromagnetic power transferred back from the SWNT to the substrate:

$$P^{\text{nt}\rightarrow\text{sub}} = \int_{V_{sub}} d\mathbf{R}_{sub} \langle \mathbf{j}^{\text{in, nt}}(\mathbf{R}_{sub}, t) \cdot \mathbf{E}^{\text{nt}}(\mathbf{R}_{sub}, t) \rangle \quad (7)$$

We expand fluctuating electromagnetic fields and induced electric currents into Fourier integrals $f(\mathbf{r},t) = \int_{-\infty}^{\infty} d\omega f(\mathbf{r},\omega)$ and make use of the constitutive equations for both surfaces: $\mathbf{j}^{\text{in},\mathscr{A}}(\mathbf{r},\omega) = \underline{\underline{\sigma}}^{\mathscr{A}}(\omega) \cdot \mathbf{E}^{\mathscr{A}}(\mathbf{r},\omega)$, where $\mathscr{A}$ = sub or nt. The conductivity

tensor is $\sigma^{nt}_{\alpha\beta}(\omega) = \delta_{\alpha z}\delta_{\beta z}\sigma_{zz}(\omega)$ for the SWNT, $\sigma^{sub}_{\alpha\beta}(\omega) = (\varepsilon_{sub}(\omega) - 1)\delta_{\alpha\beta}\omega/4i\pi$ for the substrate. Though electromagnetic response of the SWNT is anisotropic, one can neglect all components of the SWNT conductivity tensor but the axial one, $\sigma_{zz}(\omega)$, thus emphasizing the quasi one-dimensional response of the SWNT.

Then the heat flux can be written as $\dot{Q} = \int_0^\infty d\omega \dot{q}(\omega)$, where

$$\dot{q}(\omega) = 2N\mathrm{Re}\sigma_{zz}(\omega)\int_{S_{nt}} d\mathbf{R}_{nt}\{E_z^{sub}(\mathbf{R}_{nt},\omega)E_z^{sub*}(\mathbf{R}_{nt},\omega)\} - \frac{N\omega\mathrm{Im}\varepsilon_{sub}(\omega)}{2\pi}\int_{V_{sub}} d\mathbf{R}_S \sum_{\alpha=x,y,z}\{E_\alpha^{nt}(\mathbf{R}_S,\omega)\mathbf{E}_\alpha^{nt*}(\mathbf{R}_S,\omega)\} \quad (8)$$

is the heat spectral density. Here the cross-spectral density $\{E_\alpha(\mathbf{r},\omega)E^*_\beta(\mathbf{r},\omega)\}$ is defined as[27] $\langle E_\alpha(\mathbf{r},\omega)E_\beta{}^*(\mathbf{r},\omega')\rangle = \delta(\omega - \omega')\{E_\alpha(\mathbf{r},\omega)E^*_\beta(\mathbf{r},\omega)\}$.

The Fourier components of the fluctuating fields in the system are given by[54,55]

$$\mathbf{E}^{\mathscr{l}}(\mathbf{r},\omega) = (i\omega/c^2)\int d\mathbf{R}_A \underline{\underline{G}}(\mathbf{r},\mathbf{R}_{\mathscr{l}},\omega)\cdot\mathbf{j}^{\mathscr{l}}(\mathbf{R}_A,\omega) \quad (9)$$

where $\underline{\underline{G}}$ is the Green dyadic of the metallic SWNT placed above the dielectric substrate, and the integral is taken over the region containing fluctuating current sources, that is, the SWNT surface S_{nt} or the substrate volume V_{sub}. According to the fluctuation–dissipation theorem,[27,28,35] in the linear response regime,[56] the cross-spectral densities of these currents are defined as

$$\{j_\alpha^{\mathscr{l}}(\mathbf{R}_{\mathscr{l}},\omega)j^{*\mathscr{l}}_\beta(\mathbf{R}'_{\mathscr{l}},\omega)\} = (1/\pi)\Theta(\omega,T_{\mathscr{l}})\mathrm{Re}\sigma^{\mathscr{l}}_{\alpha\beta}(\omega)\delta(\mathbf{R}_{\mathscr{l}} - \mathbf{R}'_{\mathscr{l}}) \quad (10)$$

where the blackbody thermal function is $\Theta(\omega,T) = \hbar\omega/(\exp(\hbar\omega/k_BT) - 1)$, k_B is the Boltzmann constant, and $\alpha,\beta = x,y,z$. Hereinafter, we assume that both the substrate and the SWNT are in the local thermodynamic equilibrium at the temperatures T_{sub} and T_{nt}, respectively. Substituting these expressions into eq 8, we obtain the following expression for the spectral heat flux:

$$\dot{q}(\omega) = \frac{N\omega^3\mathrm{Re}\sigma_{zz}(\omega)\mathrm{Im}\varepsilon_{sub}(\omega)}{2\pi^2c^4}(\Theta(\omega,T_{sub}) - \Theta(\omega,T_{nt})) \times \int_{S_{nt}} d\mathbf{R}_{nt}\int_{V_{sub}} d\mathbf{R}_{sub}\sum_{\alpha=x,y,z}|G_{\alpha z}(\mathbf{R}_{sub},\mathbf{R}_{nt},\omega)|^2 \quad (11)$$

The electric Green dyadic, $\underline{\underline{G}}(\mathbf{r},\mathbf{r}',\omega)$, for an individual SWNT placed above the dielectric substrate is defined as

$$[(\nabla_{\mathbf{r}}\times\underline{\underline{I}})\cdot(\nabla_{\mathbf{r}}\times\underline{\underline{I}}) - k^2(\mathbf{r})\underline{\underline{I}}]\cdot\underline{\underline{G}}(\mathbf{r},\mathbf{r}',\omega) = 4\pi\underline{\underline{I}}\delta(\mathbf{r}-\mathbf{r}') \quad (12)$$

where

$$k(\mathbf{r}) = \begin{cases}(\omega/c)\sqrt{\varepsilon_{sub}}, & z<0\\ (\omega/c), & z>0\end{cases} \quad (13)$$

is the wavenumber, $\underline{\underline{I}}$ is the unit dyadic, $\delta(\mathbf{r}-\mathbf{r}')$ is the Dirac delta function. The Green dyadic $\underline{\underline{G}}$ must also satisfy boundary conditions imposed on the SWNT surface (see eqs 7 and 8 in ref 42). Using vector Green theorem, we reduce eq 12 to the Hallen integral equation for the Green dyadic, which is numerically solved then (see refs 40–42 and Supporting Information for details).

Conflict of Interest: The authors declare no competing financial interest.

Acknowledgment. This work was supported by DoD (AFOSR FA9550-11-1-0185) and Lehigh University (Faculty Innovation Grant).

Supporting Information Available: Details of derivation of the expression for heat flux between SWNT forest and dielectric substrate, interface thermal conductance dependence on a radius of metallic SWNTs in the forest, thermal conductance across a gap between a forest of semiconducting SWNTs and quartz substrate. This material is available free of charge *via* the Internet at http://pubs.acs.org.

REFERENCES AND NOTES

1. *The International Technology Roadmap for Semiconductors*, 2011.
2. Balandin, A. Thermal Properties of Graphene and Nanostructured Carbon Materials. *Nat. Mater.* **2011**, *10*, 569–581.
3. Huxtable, S. T.; Cahill, D. G.; Shenogin, S.; Xue, L.; Ozisik, R.; Barone, P.; Usrey, M.; Strano, M. S.; Siddons, G.; Shim, M.; *et al.* Interfacial Heat Flow in Carbon Nanotube Suspensions. *Nat. Mater.* **2003**, *2*, 731–734.
4. Maune, H.; Chiu, H.-Y.; Bockrath, M. Thermal Resistance of the Nanoscale Constrictions between Carbon Nanotubes and Solid Substrates. *Appl. Phys. Lett.* **2006**, *89*, 013109.
5. Pop, E.; Mann, D. A.; Goodson, K. E.; Dai, H. Electrical and Thermal Transport in Metallic Single-Wall Carbon Nanotubes on Insulating Substrates. *J. Appl. Phys.* **2007**, *101*, 093710.
6. Tsen, A. W.; Donev, L. A. K.; Kurt, H.; Herman, L. H.; Park, J. Imaging the Electrical Conductance of Individual Carbon Nanotubes with Photothermal Current Microscopy. *Nat. Nanotechnol.* **2009**, *4*, 108–113.
7. Shi, L.; Zhou, J.; Kim, P.; Bachtold, A.; Majumdar, A.; McEuen, P. L. Thermal Probing of Energy Dissipation in Current-Carrying Carbon Nanotubes. *J. Appl. Phys.* **2009**, *105*, 104306.
8. Baloch, K. H.; Voskanian, N.; Cumings, J. Controlling the Thermal Contact Resistance of a Carbon Nanotube Heat Spreader. *Appl. Phys. Lett.* **2010**, *97*, 063105.
9. Tsai, C.-L.; Liao, A.; Pop, E.; Shim, M. Electrical Power Dissipation in Semiconducting Carbon Nanotubes on Single Crystal Quartz and Amorphous SiO_2. *Appl. Phys. Lett.* **2011**, *99*, 053120.
10. Hirotani, J.; Ikuta, T.; Nishiyama, T.; Takahashi, K. Thermal Boundary Resistance between the End of an Individual Carbon Nanotube and a Au Surface. *Nanotechnology* **2011**, *22*, 315702.
11. Xu, J.; Fisher, T. S. Enhancement of Thermal Interface Materials with Carbon Nanotube Arrays. *Int. J. Heat Mass Transfer* **2006**, *49*, 1658–1666.
12. Cola, B. A.; Xu, X.; Fisher, T. S. Increased Real Contact in Thermal Interfaces: A Carbon Nanotube/Foil Material. *Appl. Phys. Lett.* **2007**, *90*, 093513.
13. Tong, T.; Zhao, Y.; Delzeit, L.; Kashani, A.; Meyyappan, M.; Majumdar, A. Dense Vertically Aligned Multiwalled Carbon Nanotube Arrays as Thermal Interface Materials. *IEEE Trans. Compon., Packag. Technol.* **2007**, *30*, 92–100.
14. Panzer, M. A.; Zhang, G.; Mann, D.; Hu, X.; Pop, E.; Dai, H.; Goodson, K. E. Thermal Properties of Metal-Coated Vertically Aligned Single-Wall Nanotube Arrays. *J. Heat Transfer* **2008**, *130*, 052401.
15. Zhang, K.; Chai, Y.; Yuen, M. M. F.; Xiao, D. G. W.; Chan, P. C. H. Carbon Nanotube Thermal Interface Material for High-Brightness Light-Emitting-Diode Cooling. *Nanotechnology* **2008**, *19*, 215706.
16. Li, Q.; Liu, C.; Fan, S. Thermal Boundary Resistances of Carbon Nanotubes in Contact with Metals and Polymers. *Nano Lett.* **2009**, *9*, 3805–3809.
17. Yang, J.; Yang, Y.; Waltermire, S. W.; Gutu, T.; Zinn, A. A.; Xu, T. T.; Chen, Y.; Li, D. Measurement of the Intrinsic Thermal Conductivity of a Multiwalled Carbon Nanotube and Its Contact Thermal Resistance with the Substrate. *Small* **2011**, *7*, 2334–2340.
18. Hu, M.; Keblinski, P.; Wang, J.-S.; Raravikar, N. Interfacial Thermal Conductance between Silicon and a Vertical Carbon Nanotube. *J. Appl. Phys.* **2008**, *104*, 083503.
19. Carlborg, C. F.; Shiomi, J.; Maruyama, S. Thermal Boundary Resistance between Single-Walled Carbon Nanotubes and Surrounding Matrices. *Phys. Rev. B* **2008**, *78*, 205406.
20. Rotkin, S. V.; Perebeinos, V.; Petrov, A. G.; Avouris, P. An Essential Mechanism of Heat Dissipation in Carbon Nanotube Electronics. *Nano Lett.* **2009**, *9*, 1850–1855.
21. Cola, B. A.; Xu, J.; Fisher, T. S. Contact Mechanics and Thermal Conductance of Carbon Nanotube Array Interfaces. *Int. J. Heat Mass Transfer* **2009**, *52*, 3490–3503.
22. Fan, H.-B.; Zhang, K.; Yuen, M. M. F. The Interfacial Thermal Conductance between a Vertical Single-Wall Carbon

Nanotube and a Silicon Substrate. *J. Appl. Phys.* **2009**, *106*, 034307.
23. Ong, Z.-Y.; Pop, E. Molecular Dynamics Simulation of Thermal Boundary Conductance between Carbon Nanotubes and SiO_2. *Phys. Rev. B* **2010**, *81*, 155408.
24. Gao, F.; Qu, J.; Yao, M. Interfacial Thermal Resistance between Metallic Carbon Nanotube and Cu Substrate. *J. Appl. Phys.* **2011**, *110*, 124314.
25. Polder, D.; Van Hove, M. Theory of Radiative Heat Transfer between Closely Spaced Bodies. *Phys. Rev. B* **1971**, *4*, 3303–3314.
26. Domingues, G.; Volz, S.; Joulain, K.; Greffet, J.-J. Heat Transfer between Two Nanoparticles through Near Field Interaction. *Phys. Rev. Lett.* **2005**, *94*, 085901.
27. Joulain, K.; Mulet, J.-P.; Marquier, F.; Carminati, R.; Greffet, J.-J. Surface Electromagnetic Waves Thermally Excited: Radiative Heat Transfer, Coherence Properties and Casimir Forces Revisited in the Near Field. *Surf. Sci. Rep.* **2005**, *57*, 59–112.
28. Volokitin, A. I.; Persson, B. N. J. Near-Field Radiative Heat Transfer and Noncontact Friction. *Rev. Mod. Phys.* **2007**, *79*, 1291–1329.
29. Narayanaswamy, A.; Shen, S.; Chen, G. Near-Field Radiative Heat Transfer between a Sphere and a Substrate. *Phys. Rev. B* **2008**, *78*, 115303.
30. Volokitin, A. I.; Persson, B. N. J. Near-Field Radiative Heat Transfer between Closely Spaced Graphene and Amorphous SiO_2. *Phys. Rev. B* **2011**, *83*, 241407.
31. Mahan, G. D. The Tunneling of Heat. *Appl. Phys. Lett.* **2011**, *98*, 132106.
32. Rousseau, E.; Siria, A.; Jourdan, G.; Volz, S.; Comin, F.; Chevrier, J.; Greffet, J.-J. Radiative Heat Transfer at the Nanoscale. *Nat. Photonics* **2009**, *3*, 514–517.
33. Shen, S.; Narayanaswamy, A.; Chen, G. Surface Phonon Polaritons Mediated Energy Transfer between Nanoscale Gaps. *Nano Lett.* **2009**, *9*, 2909–2913.
34. Ottens, R. S.; Quetschke, V.; Wise, S.; Alemi, A. A.; Lundock, R.; Mueller, G.; Reitze, D. H.; Tanner, D. B.; Whiting, B. F. Near-Field Radiative Heat Transfer between Macroscopic Planar Surfaces. *Phys. Rev. Lett.* **2011**, *107*, 014301.
35. Rytov, S. M.; Kravtsov, I. A.; Tatarskii, V. I. *Principles of Statistical Radiophysics*; Springer-Verlag: Berlin, 1989; Vol. 3.
36. Hafeli, A. K.; Rephaeli, E.; Fan, S.; Cahill, D. G.; Tiwald, T. E. Temperature Dependence of Surface Phonon Polaritons from a Quartz Grating. *J. Appl. Phys.* **2011**, *110*, 043517.
37. Surface plasmons in neighboring SWNTs are very weakly electromagnetically coupled in our case with negligible change in plasmonic local density of states. The criterion for weak coupling was established in our previous work.[42]
38. Hu, M.; Shenogin, S.; Keblinski, P.; Raravikar, N. Thermal Energy Exchange between Carbon Nanotube and Air. *Appl. Phys. Lett.* **2007**, *90*, 231905.
39. Hsu, I.-K.; Pettes, M. T.; Aykol, M.; Chang, C.-C.; Hung, W.-H.; Theiss, J.; Shi, L.; Cronin, S. B. Direct Observation of Heat Dissipation in Individual Suspended Carbon Nanotubes Using a Two-Laser Technique. *J. Appl. Phys.* **2011**, *110*, 044328.
40. Nemilentsau, A. M.; Slepyan, G. Y.; Maksimenko, S. A. Thermal Radiation from Carbon Nanotubes in the Terahertz Range. *Phys. Rev. Lett.* **2007**, *99*, 147403.
41. Nemilentsau, A. M.; Slepyan, G. Y.; Maksimenko, S. A.; Lakhtakia, A.; Rotkin, S. V. Spontaneous Decay of the Excited State of an Emitter near a Finite-Length Metallic Carbon Nanotube. *Phys. Rev. B* **2010**, *82*, 235411.
42. Nemilentsau, A.; Slepyan, G.; Maksimenko, S.; Lakhtakia, A.; Rotkin, S. V. Spontaneous Decay of an Excited State of an Emitter Coupled to Parallel SWNTs Placed in the Vicinity of a Plane Interface between Two Dielectric Materials. *Photonics Nanostruct.* **2011**, *9*, 381–389.
43. Slepyan, G. Ya.; Maksimenko, S. A.; Lakhtakia, A.; Yevtushenko, O.; Gusakov, A. V. Electrodynamics of Carbon Nanotubes: Dynamic Conductivity, Impedance Boundary Conditions, and Surface Wave Propagation. *Phys. Rev. B* **1999**, *60*, 17136–17149.
44. Nemilentsau, A. M. Tutorial: Linear Surface Conductivity of an Achiral Single-Wall Carbon Nanotube. *J. Nanophotonics* **2011**, *5*, 050401.
45. Spitzer, W. G.; Kleinman, D. A. Infrared Lattice Bands of Quartz. *Phys. Rev.* **1961**, *121*, 1324–1335.
46. Duarte, J. L.; Sanjurjo, J. A.; Katiyar, R. S. Off-Normal Infrared Reflectivity in Uniaxial Crystals: α-$LiIO_3$ and α-Quartz. *Phys. Rev. B* **1987**, *36*, 3368–3372.
47. Quartz dielectric function for the ordinary ray is used here. In general, the electromagnetic response is anisotropic in quartz. However, main conclusions of the simplified isotropic model are also valid for a general anisotropic case.
48. Hanson, G. Fundamental Transmitting Properties of Carbon Nanotube Antennas. *IEEE Trans. Antennas Propag.* **2005**, *53*, 3426–3435.
49. Slepyan, G. Y.; Shuba, M. V.; Maksimenko, S. A.; Lakhtakia, A. Theory of Optical Scattering by Achiral Carbon Nanotubes and Their Potential as Optical Nanoantennas. *Phys. Rev. B* **2006**, *73*, 195416.
50. Volokitin, A. I.; Persson, B. N. J. Radiative Heat Transfer between Nanostructures. *Phys. Rev. B* **2001**, *63*, 205404.
51. Rousseau, E.; Laroche, M.; Greffet, J.-J. Asymptotic Expressions Describing Radiative Heat Transfer between Polar Materials from the Far-Field Regime to the Nanoscale Regime. *J. Appl. Phys.* **2012**, *111*, 014311.
52. We define partial conductance as: $g(\omega_1{:}\omega_2) = \int_{\omega_1}^{\omega_2} g(\omega)\mathrm{d}\omega$.
53. The plasmon contribution to the thermal Kapitza conductance is approximately the same for the forest of zigzag (15,0) SWNTs (radius 0.59 nm) and armchair (10,10) SWNTs (radius 0.68 nm).
54. Novotny, L.; Hecht, B. *Principles of Nano-Optics*; Cambridge University Press: Cambridge, 2006.
55. Nemilentsau, A. M.; Slepyan, G. Ya.; Maksimenko, S. A.; Lakhtakia, A.; Rotkin, S. V. Scattering of the Near Field of an Electric Dipole by a Single-Wall Carbon Nanotube. *J. Nanophotonics* **2010**, *4*, 041685.
56. The linear regime requires the thermal functions of the substrate and the forest to be sufficiently independent.